

Downpour Dynamics: Outsized impacts of storm events on unprocessed atmospheric nitrate export in an urban watershed

Joel T. Bostic^{1,2}, David M. Nelson¹, Keith N. Eshleman¹

¹University of Maryland Center for Environmental Science, Appalachian Lab, Frostburg, Maryland, USA

²[Garrett College, McHenry, MD, USA](#)

Correspondence to: Joel Bostic (jbostic@umces.edu)

Abstract. Water-quality impacts of streamwater nitrate (NO_3^-) on downstream ecosystems are largely determined by the load of NO_3^- from the watershed to surface waters. The largest NO_3^- loads often occur during storm events, but it is unclear how loads of different NO_3^- sources change during storm events relative to baseflow or how watershed attributes might affect source export. To assess the role of stormflow and baseflow on NO_3^- source export and how these roles are modulated by hydrologic effects of land-use practices, we measured nitrogen ($\delta^{15}\text{N}$) and oxygen ($\Delta^{17}\text{O}$) isotopes of NO_3^- and oxygen isotopes ($\delta^{18}\text{O}$) of water in rainfall and streamwater samples from before, during, and after eight storm events across 14 months in two Chesapeake Bay watersheds of contrasting land-use. Storms had a disproportionately large influence on the export of unprocessed atmospheric NO_3^- ($\text{NO}_3^-_{\text{Atm}}$) and a disproportionately small influence on export of terrestrial NO_3^- ($\text{NO}_3^-_{\text{Terr}}$) relative to baseflow in the developed urban watershed. In contrast, baseflow and stormflow had similar influences on $\text{NO}_3^-_{\text{Atm}}$ and $\text{NO}_3^-_{\text{Terr}}$ export in the mixed agricultural/forested watershed. An equivalent relationship between $\text{NO}_3^-_{\text{Atm}}$ deposition on impervious surfaces and event $\text{NO}_3^-_{\text{Atm}}$ streamwater export in the urban watershed suggests that impervious surfaces that hydrologically connect runoff to channels likely facilitate export of $\text{NO}_3^-_{\text{Atm}}$ during rainfall events. Additionally, larger rainfall events were more effective in exporting $\text{NO}_3^-_{\text{Atm}}$ in the urban watershed, with increased rainfall depth resulting in a greater fraction of event $\text{NO}_3^-_{\text{Atm}}$ deposition exported. Considering both projected increases in precipitation amounts and intensity and urban/suburban sprawl in many regions of the world, best management practices that reduce hydrologic connectivity of impervious surfaces will likely help to mitigate the impact of storm events on $\text{NO}_3^-_{\text{Atm}}$ export from developed watersheds.

29 **1 Introduction**

30 Increasing streamwater nitrate (NO_3^-) export over the past century has negatively impacted
31 many downstream ecosystems globally (Kemp et al., 2005; Camargo and Alonso, 2006; Steffen et al.,
32 2015; Stevens, 2019). The severity of impacts to receiving waters is partially determined by the
33 magnitude of NO_3^- loads (i.e., product of concentration and discharge; NRC, 2000). As such, riverine
34 NO_3^- loads are greatest during periods of high discharge, which often follow large precipitation events,
35 and can therefore have an outsized impact on annual streamwater NO_3^- loads (Vaughan et al., 2017;
36 Kincaid et al., 2020). Sources of NO_3^- comprising storm event loads can be variable and associated with
37 changing hydrologic flowpaths during precipitation events (Buda and DeWalle, 2009). Exported loads
38 of individual NO_3^- sources (e.g., atmospheric NO_3^-) are less often quantified during storm events than
39 routine baseflow samples, however (Divers et al., 2014; Sabo et al., 2016). Thus, it is not clear whether
40 storm events have a disproportionate impact relative to non-storm (i.e., baseflow) conditions on different
41 NO_3^- sources. The impact of storm events relative to baseflow on sources of streamwater NO_3^- is
42 particularly relevant given the increases in precipitation amount and intensity projected to be associated
43 with future climate change (Walsh et al., 2014).

44 Precipitation can affect the amount, as well as the source, of NO_3^- exported in surface waters
45 via the surface-to-stream flow path. During storms, NO_3^- can be transported to streams by either
46 overland or subsurface pathways. Overland flow is associated with NO_3^- sources deposited or present
47 on the land surface, such as unprocessed atmospheric NO_3^- ($\text{NO}_3^-_{\text{Atm}}$; Rose et al., 2015a). Subsurface
48 flow is associated with NO_3^- sources abundant in soils and groundwater, such as fertilizer, microbial,
49 and/or sewage (Cook and Herczeg, 2012). Both hydrologic flowpaths (and the respective NO_3^- sources)
50 can be affected by human land-use activities (Paul and Meyer, 2001; Barnes and Raymond, 2010; Jarvis,
51 2020). For example, previous studies report that developed watersheds export relatively more $\text{NO}_3^-_{\text{Atm}}$
52 than less developed watersheds, presumably due to hydrologic changes created by impervious surfaces
53 (Buda and DeWalle, 2009; Burns et al., 2009; Kaushal et al., 2011; Bostic et al., 2021). However,
54 evidence is lacking for (1) the mechanism generating increased $\text{NO}_3^-_{\text{Atm}}$ export in developed watersheds
55 and (2) quantitative impacts of storm event loads relative to baseflow, both of which could be useful for
56 mitigating the effects of storms on streamwater NO_3^- export.

57 The stable isotope compositions of NO_3^- and water (H_2O) are powerful tools for distinguishing
58 NO_3^- sources and hydrologic flow paths, respectively. For example, the oxygen isotope values ($\Delta^{17}\text{O}$)
59 of NO_3^- allow for quantification of atmospheric and terrestrial sources of NO_3^- in streamwater
60 (Michalski et al., 2003), and $\delta^{15}\text{N}$ and $\delta^{18}\text{O}$ values of NO_3^- permit inferences into the relative
61 contributions of terrestrially-sourced NO_3^- ($\text{NO}_3^-_{\text{Terr}}$), such as fertilizer or sewage N (Kendall et al.,
62 2007). Additionally, $\delta^{18}\text{O}$ values of H_2O can be used to assess the importance of overland versus
63 subsurface flow through partitioning of stream flow into pre-event and event contributions (Sklash et al.,
64 1976; McGuire and McDonnell, 2007). Few studies have coupled these isotopic tracers (Buda and
65 DeWalle, 2009), however, despite their suitability to assess the effect of storm events on both hydrologic
66 flow paths and export of different NO_3^- sources. Such information could provide mechanistic evidence
67 for the commonly reported relationship between developed watersheds and $\text{NO}_3^-_{\text{Atm}}$ export.

68 Here we address the following research questions: How do storm events affect the total amount
69 and sources of NO_3^- exported in streams relative to baseflow? And, more specifically, what is the
70 relationship between hydrologic and biogeochemical effects of land use and the export of unprocessed
71 atmospheric $\text{NO}_3^-_{\text{Atm}}$ and terrestrial NO_3^- during storm events and baseflow? These questions were
72 addressed in two Chesapeake Bay watersheds of contrasting land-use. A two-watershed study is
73 inherently comparative, potentially limiting the inferences that can be made regarding land-use effects.
74 However, given the contrasting land uses (i.e., predominantly developed compared to mixed
75 forest/agriculture) in these watersheds, we believe that this study can adequately address our research
76 questions while presenting a “proof of concept” for future studies. To address these research questions,
77 we collected moderate-frequency (45 minute – 12 hour) streamwater samples before, during, and after
78 eight rainfall events, bulk rainfall samples corresponding to these events, as well as monthly baseflow
79 samples, in two catchments within the broader Chesapeake Bay watershed. We then used $\delta^{15}\text{N}$, $\delta^{18}\text{O}$,
80 and $\Delta^{17}\text{O}$ of NO_3^- and $\delta^{18}\text{O}$ of H_2O to determine NO_3^- sources and hydrologic flowpaths, respectively.
81 The Chesapeake Bay region is ideal for our study: it is one of the most ecologically and economically
82 important estuaries in the world (NOAA, 1990) that has experienced recent improvements in ecosystem
83 health associated with declining N loads (Chanat et al., 2016; Lefcheck et al., 2018; Zhang et al., 2018),

84 but uncertainty surrounds continued water quality improvements in part due to the effects of projected
85 increases in precipitation intensity across its diverse land-use watershed (Najjar et al., 2010).

86 **2 Materials and Methods**

87 **2.1 Study watersheds and field methods**

88 To assess NO_3^- export dynamics during storm events, streamwater and rainfall samples were
89 collected synchronously during eight events from two watersheds with outlets in Maryland, USA –
90 Gwynns Falls at Villa Nova (GWN) and Gunpowder Falls at Glencoe (GUN) (Figure 1) – from
91 September 2018 – October 2019. These watersheds have similar geology (Piedmont physiographic
92 province; Fenneman, 1946) and climate (humid sub-tropical; Kottek et al., 2006), but differing land-use
93 (one predominantly developed and the other mixed forest and agriculture), impervious surface coverage
94 (Figure S1) and area (Table 1). Events were targeted based on forecast precipitation amounts of at least
95 2.5 cm and the same events were sampled at each site. Automated samplers (Teledyne ISCO 3700
96 Portable Sampler, Lincoln, NE) were used to collect streamwater samples into pre-cleaned 1L bottles
97 across each storm hydrograph, including pre-storm baseflow, rising limbs, and falling limbs for most
98 events at intervals ranging from 45 minutes – 12 hours (Figure S2). A pre-event baseflow sample was
99 not collected for the first storm, thus any figures or analyses that compare pre-event baseflow to event
100 mean concentrations or event-water fractions have seven data points. Storm sample collection ceased
101 when discharge fell to approximately 200% of pre-event baseflow. Bulk rainfall samples corresponding
102 to each event were collected using 7.5 cm diameter funnels approximately 1 m above ground level
103 connected to pre-cleaned 1 L Nalgene bottles, with pre-cleaned table tennis balls used to limit
104 evaporation. Streamwater and rainfall samples were placed on ice for 12 – 36 hours after collection, then
105 processed in the laboratory within 24 – 48 hours. Both study watersheds are gaged by the United States
106 Geological Survey; 15-minute and mean daily discharge data were obtained using the dataRetrieval R
107 package (DeCicco, 2018). Mean event rainfall depth for each watershed was obtained from PRISM
108 Climate Group (PRISM, 2014) using the prism R package (Hart and Bell, 2015).

109 **2.2 Lab Methods**

110 Streamwater and rainfall samples for NO_3^- concentration and isotope analyses were filtered (0.45 μm)
111 and frozen within 48 hours of collection. Aliquots for water isotope measurements were stored in
112 completely filled (i.e., no headspace) 20 mL bottles at room temperature prior to analysis. NO_3^- and
113 nitrite (NO_2^-) concentrations were measured using flow-injection colorimetric analysis (Lachat
114 Quikchem 8000 FIA+).

115 The $\Delta^{17}\text{O}$, $\delta^{18}\text{O}$, and $\delta^{15}\text{N}$ values of stream and rainfall NO_3^- were measured using a Thermo
116 Delta V+ isotope ratio mass spectrometer (Bremen, Germany) via the denitrifier method (Sigman et al.,
117 2001; Casciotti et al., 2002) with thermal decomposition (at 800° C) of N_2O to N_2 and O_2 (Kaiser et al.,
118 2007) at the Central Appalachians Stable Isotope Facility. NO_2^- is denitrified using this method as well,
119 but NO_2^- concentrations in stream and rainfall samples were low relative to NO_3^- ($\text{NO}_2^-/(\text{NO}_2^- + \text{NO}_3^-)$
120 mean = 0.006, range = 0.00 – 0.027). Measured isotope ratios were normalized using international
121 reference standards USGS 34 ($\delta^{17}\text{O} = -14.8 \text{‰}$, $\delta^{18}\text{O} = -27.9 \text{‰}$) and USGS 35 ($\delta^{17}\text{O} = 51.5 \text{‰}$, $\delta^{18}\text{O} =$
122 57.5‰) for O isotopes (Böhlke et al., 2003) and USGS 32 ($\delta^{15}\text{N} = 180 \text{‰}$) and USGS 34 ($\delta^{15}\text{N} = -1.8$
123 ‰) for N isotopes (IAEA, 1995). Reference standards were measured throughout sample analysis in
124 equal concentrations to samples (ranging from 100 – 200 nmol depending on sample NO_3^-
125 concentration). Analytical precision of $\Delta^{17}\text{O}$ ($\Delta^{17}\text{O} \approx \delta^{17}\text{O} - 0.52 \times \delta^{18}\text{O}$) was estimated as 0.5 ‰ , $\delta^{18}\text{O}$
126 as 1.4 ‰ , and $\delta^{15}\text{N}$ as 1.8 ‰ (1 σ), based on repeated measurements ($n \approx 200$) of reference standards
127 USGS 32 and USGS 35 and a laboratory reference standard “Chile NO_3^- ” (Duda Energy 1sn 1 lb.
128 Sodium Nitrate Fertilizer 99+% Pure Chile Saltpeter from Amazon.com). Accuracy of $\Delta^{17}\text{O}$, $\delta^{18}\text{O}$, and
129 $\delta^{15}\text{N}$ were tracked using repeated measurements of IAEA-N3 ($n = 19$, mean $\Delta^{17}\text{O} = -0.1 \text{‰}$, $\delta^{18}\text{O} = 24.3$
130 ‰ , $\delta^{15}\text{N} = 4.5 \text{‰}$) and closely agreed with published values (IAEA, 1995; Michalski et al., 2002; Böhlke
131 et al., 2003). Each streamwater and rainfall sample was measured 3 – 6 times to reduce analytical
132 uncertainty and the mean of each sample was used in all analyses. Standard error of the mean ranged
133 from 0.1 – 0.6 ‰ , 0.1 – 1.6 ‰ , and 0.1 – 1.6 ‰ for replicate measurements of $\Delta^{17}\text{O}$, $\delta^{18}\text{O}$, and $\delta^{15}\text{N}$
134 respectively.

135 Oxygen ($\delta^{18}\text{O}_{\text{H}_2\text{O}}$) isotopes of rainfall and streamwater were measured using a Picarro L2130-
 136 i via cavity ring down spectroscopy at the University of Wyoming Stable Isotope Facility. Measured
 137 isotope ratios were normalized to VSMOW using internal laboratory standards that were calibrated to
 138 international standards. Precision based on repeated measurements of internal standards was 0.2 ‰.

139 2.3 Quantification of atmospheric NO_3^- deposition

140 Event NO_3^- Atm deposition was quantified using the measured rainfall NO_3^- concentration and
 141 mean rainfall depth (Lovett et al., 2000; Nelson et al., 2018; Huang et al., 2020):

$$142 \text{NO}_3^- \text{Atm Deposition (g N ha}^{-1}\text{)} = \frac{\text{Rainfall Volume (L)} \times \text{Rainfall NO}_3^- \text{(mg N L}^{-1}\text{)}}{\text{Watershed Area (ha)}} \times (1 \times 10^{-3}) \text{ (eq.}$$

143 1)

144 where rainfall volume is the product of rainfall depth and watershed area and 1×10^{-3} is a conversion
 145 factor. Event NO_3^- Atm deposition onto impervious surfaces was then calculated by multiplying NO_3^- Atm
 146 deposition by the percent of impervious surfaces.

147 2.4 Quantification of unprocessed atmospheric and terrestrial NO_3^- in streams

148 Concentrations of NO_3^- Atm were quantified using $\Delta^{17}\text{O}$ values of terrestrial and rainfall end-
 149 members and total NO_3^- concentrations:

$$150 f_{\text{Atm}} = \frac{(\Delta^{17}\text{O}_{\text{Stream}} - \Delta^{17}\text{O}_{\text{Terr}})}{(\Delta^{17}\text{O}_{\text{Precip}} - \Delta^{17}\text{O}_{\text{Terr}})} \quad \text{(eq. 2)}$$

$$151 \text{NO}_3^- \text{Atm (mg N L}^{-1}\text{)} = f_{\text{Atm}} \times \text{NO}_3^- \text{Total (mg N L}^{-1}\text{)} \quad \text{(eq. 3)}$$

$$152 \text{NO}_3^- \text{Terr (mg N L}^{-1}\text{)} = \text{NO}_3^- \text{Total (mg N L}^{-1}\text{)} - \text{NO}_3^- \text{Atm (mg N L}^{-1}\text{)} \quad \text{(eq. 4)}$$

153 where $\Delta^{17}\text{O}_{\text{Stream}} = \Delta^{17}\text{O}$ of streamwater samples during either baseflow or storm events, $\Delta^{17}\text{O}_{\text{Precip}} = \Delta^{17}\text{O}$
 154 of rainfall for a given event, $\Delta^{17}\text{O}_{\text{Terr}} = \Delta^{17}\text{O}$ of terrestrially sourced NO_3^- which is $\cong 0$ ‰, NO_3^- Terr =
 155 terrestrial NO_3^- , and NO_3^- Total = measured streamwater NO_3^- concentrations. Uncertainty in NO_3^- Atm
 156 was estimated by propagating analytical uncertainty from repeated measures of $\Delta^{17}\text{O}_{\text{Stream}}$ and $\Delta^{17}\text{O}_{\text{Precip}}$.

157 2.5 Quantification of event loads and mean concentrations and monthly loads

158 Event loads of NO_3^- Total and NO_3^- Atm were calculated as:

$$159 L_{\text{NO}_3^-} = \sum_{i=1}^n C_i \times V_i \times (1 \times 10^{-3}) \quad \text{(eq. 5)}$$

160 where L = load of either NO_3^- Total, NO_3^- Atm, or NO_3^- Terr in g per event, C_i = concentration of either NO_3^-
 161 Total or NO_3^- Atm in mg N L^{-1} for sample i , and V_i = volume of water exported corresponding to sample i
 162 in L, and 1×10^{-3} is a conversion factor (mg to g). Event yields ($\text{g N ha}^{-1} \text{ event}^{-1}$) of NO_3^- Total, NO_3^- Atm,
 163 and NO_3^- Terr were calculated by normalizing loads by watershed area. To assess potential bias in NO_3^- Atm
 164 load quantification between our method (i.e., multiple samples collected during a storm event; eq. 5) and
 165 methods in which a single sample is collected, we multiplied the mean daily discharge by NO_3^- Atm
 166 concentrations of each individual grab sample collected during a particular event. We compared these
 167 estimated loads with the “true” load (calculated using eq. 5) and calculated bias as the difference between
 168 the “true” load and loads estimated using a single sample and daily average discharge. Because
 169 traditional methods commonly use mean daily discharge, we only investigated bias for two events that
 170 included samples collected over one full day. We also calculated the event fraction of unprocessed
 171 atmospheric NO_3^- (f_{Atm}) using $\Delta^{17}\text{O}$ (eq. 2) and $\delta^{18}\text{O}$ (substituting $\delta^{18}\text{O}$ for $\Delta^{17}\text{O}$ in eq. 2 and assuming
 172 that baseflow samples for a corresponding storm represent the terrestrial NO_3^- end-member $\delta^{18}\text{O}$ value).

173 Event mean concentrations (EMC) of NO_3^- Total and NO_3^- Atm and event mean values (EMV) of
 174 $\Delta^{17}\text{O}$, $\delta^{18}\text{O}$, and $\delta^{15}\text{N}$ were calculated as:

$$175 \quad \text{EMC, EMV} = \frac{\sum_{i=1}^n (C_i \times V_i)}{\sum_{i=1}^n V_i} \quad (\text{eq. 6})$$

176 where EMC = event mean concentration in mg N L^{-1} (for NO_3^- Total and NO_3^- Atm), EMV = event mean
 177 value in ‰ ($\Delta^{17}\text{O}$, $\delta^{18}\text{O}$, and $\delta^{15}\text{N}$), C_i = either concentration of NO_3^- Total or NO_3^- Atm (mg N L^{-1}) or value
 178 of $\Delta^{17}\text{O}$, $\delta^{18}\text{O}$, or $\delta^{15}\text{N}$ (‰) corresponding to sample i , and V_i = volume of water exported corresponding
 179 to sample i (L).

180 Monthly loads of NO_3^- Total were estimated using Weighted Regressions on Time, Discharge,
 181 and Season Kalman Filter (WRTDS-K; Zhang and Hirsch, 2019). Regressions were calibrated using the
 182 entire period of record for NO_3^- (excluding our storm samples) to generate coefficients representing a
 183 greater range of hydroclimatological conditions than was realized in 13 months. NO_3^- concentration
 184 data for the entire period of record were obtained from the Chesapeake Bay Program water quality
 185 database (Chesapeake Bay Program, 2021). Our storm samples were excluded to generate similar
 186 estimates of monthly and annual loads used by monitoring agencies (e.g., Maryland Department of

187 Natural Resources, US Environmental Protection Agency) in these watersheds. Monthly yields (g N ha⁻¹) were calculated by dividing monthly loads by watershed area and monthly flow-weighted concentrations (mg N L⁻¹) were calculated by dividing monthly loads by monthly discharge. Uncertainty of NO₃⁻_{Total} was estimated using block bootstrapping methods for WRTDS-K (Zhang and Hirsch, 2019) and was propagated through all analyses using NO₃⁻_{Total} loads and/or yields.

192 The fraction of rainfall NO₃⁻ exported on an event basis was calculated as:

193
$$\text{Fraction of rainfall NO}_3^- \text{ exported} = \frac{\text{NO}_3^- \text{Atm Yield (g N ha}^{-1}\text{)}}{\text{NO}_3^- \text{Atm Deposition (g N ha}^{-1}\text{)}} \text{ (eq. 7)}$$

194 where event NO₃⁻_{Atm} deposition was calculated using eq. 1 and event NO₃⁻_{Atm} yield was calculated using eq. 5.

196 2.6 Terrestrial δ¹⁸O and δ¹⁵N calculation

197 Streamwater storm samples of δ¹⁸O and δ¹⁵N were corrected to remove the influence of NO₃⁻_{Atm} (Dejwakh et al., 2012), which has higher δ¹⁸O values and can have lower δ¹⁵N values than terrestrial NO₃⁻ (Elliott et al., 2007; Kendall et al., 2007). This was done to more carefully infer how terrestrial sources of NO₃⁻ might change during storm events, and it uses the following equations:

201
$$\delta^{15}N_{Terr} = \frac{(\delta^{15}N_{Stream} - \delta^{15}N_{Atm} \times f_{Atm})}{f_{Terr}} \quad \text{(eq. 8)}$$

202
$$\delta^{18}O_{Terr} = \frac{(\delta^{18}O_{Stream} - \delta^{18}O_{Atm} \times f_{Atm})}{f_{Terr}} \quad \text{(eq. 9)}$$

203 where δ¹⁵N/δ¹⁸O_{Stream} = measured δ¹⁵N or δ¹⁸O of streamwater storm samples, δ¹⁵N/δ¹⁸O_{Atm} = rainfall δ¹⁵N or δ¹⁸O for a given event, f_{Atm} = fraction of NO₃⁻_{Atm}, as calculated using eq. 2, and f_{Terr} = 1 - f_{Atm}.

206 2.7 Hydrograph separation

207 Water isotopes were used to quantify the proportion of event and pre-event water during storm events at or near peak discharge. The direct routing, or translation of rainfall to streamwater during the same event, was quantified as the event-water fraction (i.e., rainfall), whereas water present in the catchment prior to the storm event was classified as the pre-event water fraction (i.e., baseflow) using the following equations (Sklash et al., 1976):

212
$$f_{Event\ Water} + f_{Pre-Event\ Water} = 1 \quad (\text{eq. 9})$$

213
$$f_{Event\ Water} = \frac{\delta^{18}O_{PeakQ} - \delta^{18}O_{Baseflow}}{\delta^{18}O_{Precipitation} - \delta^{18}O_{Baseflow}} \quad (\text{eq. 10})$$

214 where $\delta^{18}O_{PeakQ} = \delta^{18}O_{H_2O}$ at or near peak discharge during storm events, $\delta^{18}O_{Baseflow} = \delta^{18}O_{H_2O}$ of
 215 streamwater just prior to storm event and hydrograph rise, and $\delta^{18}O_{Rainfall} = \delta^{18}O_{H_2O}$ of bulk rainfall
 216 samples during a given storm event. Event and pre-event water runoff can be quantified using these
 217 equations by multiplying runoff during peak stormflow by fractions of event and pre-event water.
 218 Uncertainty was estimated using published methods to account for analytical uncertainty and separation,
 219 or lack thereof, of end-members (Genereux, 1998). It has been shown that some of the assumptions of
 220 isotope-based hydrograph separation may be violated in mesoscale catchments (e.g., spatiotemporally
 221 constant end-member values; Klaus and McDonnell, 2013), thus we estimate event-water fractions and
 222 runoff for peak discharge only and apply these data cautiously.

223 **2.8 Framework for interpreting baseflow and stormflow contributions**

224 The importance of storm events relative to baseflow in streamwater NO_3^- export can be
 225 evaluated using a fractional export plot (Figure 2). In this plot the y-axis shows the fraction of annual
 226 nitrate loads exported during a single event (f_{NO_3}) and the x-axis shows the fraction of annual discharge
 227 exported during a single event (f_{Runoff}). For example, if NO_3^- concentrations remain constant with
 228 changing discharge during a storm, the data would fall on the 1:1 line because its load is perfectly
 229 explained by discharge and both storm events and baseflow have equal impact on loads (Figure 2). If
 230 NO_3^- concentrations decrease with increasing discharge during a storm, the data would plot below the
 231 1:1 line. Watersheds with events consistently plotting below the 1:1 line indicate that baseflow, relative
 232 to storm events, has an outsized impact on riverine nitrate loads. If NO_3^- concentrations increase with
 233 increasing discharge, the data would plot above the 1:1 line. Watersheds with events consistently plotting
 234 above the 1:1 line indicate that storm events have an outsized impact on riverine NO_3^- loads. This
 235 framework can be expanded further by quantifying the (potential) disproportionate effect of storm events
 236 on streamwater constituent loads relative to water yields. Dividing f_{NO_3} by f_{Runoff} provides a single value
 237 to quantify the level of disproportionality:

238
$$\text{Disproportionality Factor (DF)} = \frac{f_{\text{NO}_3^-}}{f_{\text{Runoff}}} \quad (\text{eq. 11})$$

239 *DF* can be interpreted using Figure 2: a value falling on the 1:1 line would have *DF* = 1, a value below
240 the 1:1 line would have a *DF* < 1, and a value above the 1:1 line would have *DF* > 1. For example, an
241 event with *DF* = 4 indicates that a given storm exported 4× more NO₃⁻ than water whereas an event with
242 *DF* = 0.5 indicates that a storm exported 2× less NO₃⁻ than water, after both have been normalized to
243 annual amounts.

244 **2.9 Statistical analyses**

245 All statistical tests were performed in R (R Development Core Team, 2019). A Wilcoxon
246 ranked-sum test was used to compare EMC and EMV of paired streamwater storm and baseflow samples.
247 Due to the presence of outliers, Theil-Sen slopes (calculated using the *sen* function in R) were used to
248 assess relationships between most continuous variables (Helsel et al., 2020). Least squares linear
249 regression was used when outliers were absent. Confidence intervals (95%) and p-values of Theil-Sen
250 slopes were computed using bootstrapping (10,000 replicates) to incorporate uncertainty in *DF* and
251 event-water fractions.

252 **3 Results**

253 Rainfall depth and chemistry (NO₃⁻ concentrations and isotopes, H₂O isotopes) were similar
254 between watersheds for sampled events (*p* > 0.1, Table S1). Rainfall depths ranged from 1.90 – 8.10 cm,
255 which corresponds to a range of 24-hour precipitation depth return intervals of <1 year (1-year return
256 interval ≈ 6.75 cm) up to 2-year (2-year return interval ≈ 8.3 cm) in this region (Bonnin et al., 2004).
257 Streamwater NO₃⁻ concentrations ranged from 0.05 – 0.26 mg N L⁻¹, δ¹⁵N-NO₃⁻ from -8.7 – -1.4 ‰,
258 δ¹⁸O-NO₃⁻ from 48.0 – 69.6 ‰, and Δ¹⁷O-NO₃⁻ from 13.6 – 24.9 ‰. Streamflow was slightly more
259 variable in GWN during storm events (Table S2): event mean runoff and event maximum runoff were
260 higher in GWN (*p* < 0.05 and *p* < 0.01 respectively), but event median runoff was not different between
261 the watersheds (*p* = 0.11). Across all flow conditions, NO₃⁻ concentrations were lower at GWN (median
262 = 0.78 mg N L⁻¹) than GUN (median = 2.60 mg N L⁻¹). Baseflow NO₃⁻ concentrations were higher than
263 stormflow NO₃⁻ EMCs in both watersheds, but differences were more pronounced at GWN (baseflow

264 median = 1.79 mg N L⁻¹, storm median = 0.66 mg N L⁻¹, p < 0.05) than GUN (baseflow median = 3.06
265 mg N L⁻¹, storm median = 2.55 mg N L⁻¹, p < 0.05, Figure 3 and Table S3).

266 At GWN, values of $\delta^{15}\text{N}$ were higher in baseflow (median $\delta^{15}\text{N} = 7.6$ ‰) than stormflow (EMV
267 median $\delta^{15}\text{N} = 5.0$ ‰, respectively, p < 0.05), whereas values of $\delta^{18}\text{O}-\text{NO}_3^-$ were lower in baseflow
268 (median $\delta^{18}\text{O} = 3.9$ ‰) than stormflow (EMV median $\delta^{18}\text{O} = 7.4$ ‰, p < 0.05). In contrast, values of
269 $\delta^{15}\text{N}$ - and $\delta^{18}\text{O}-\text{NO}_3^-$ did not differ between baseflow and stormflow at GUN (baseflow median $\delta^{15}\text{N} =$
270 6.2 ‰, $\delta^{18}\text{O} = 3.3$ ‰; stormflow EMV median $\delta^{15}\text{N} = 6.1$ ‰, $\delta^{18}\text{O} = 3.0$ ‰; Figure 3 and Table S3).
271 Values of $\delta^{18}\text{O}-\text{NO}_3^-_{\text{Terr}}$ were higher during baseflow at both sites (p < 0.05, Figure 3), whereas $\delta^{15}\text{N}-$
272 $\text{NO}_3^-_{\text{Terr}}$ was higher during baseflow at GWN only (p < 0.05, Figure 3). Similarly, $\Delta^{17}\text{O}$ of NO_3^- was not
273 significantly different between baseflow (median = 0.4 ‰) and stormflow (EMV median = 0.5 ‰) at
274 GUN, but was lower during baseflow (median = 0.7 ‰) than stormflow (EMV median = 2.0 ‰, p <
275 0.05, Figure 3 and Table S3) at GWN.

276 Concentrations of $\text{NO}_3^-_{\text{Terr}}$ were more temporally variable than $\text{NO}_3^-_{\text{Atm}}$. Concentrations of
277 $\text{NO}_3^-_{\text{Terr}}$ showed similar patterns to $\text{NO}_3^-_{\text{Total}}$ at both watersheds: higher during baseflow than storm
278 events (GWN baseflow median = 1.72 mg N L⁻¹, stormflow median = 0.59 mg N L⁻¹; p < 0.001, GUN
279 baseflow median = 3.03 mg N L⁻¹, stormflow median = 2.50 mg N L⁻¹; p < 0.005, Figure S3). Both GWN
280 and GUN had similar $\text{NO}_3^-_{\text{Atm}}$ concentrations between baseflow and storm events (GWN baseflow
281 median = 0.05 mg N L⁻¹, stormflow median = 0.06 mg N L⁻¹, p > 0.05, GUN baseflow median = 0.04
282 mg N L⁻¹, stormflow median = 0.06 mg N L⁻¹, p > 0.05, Figure S3).

283 Similar to NO_3^- concentrations and isotopes, $\delta^{18}\text{O}-\text{H}_2\text{O}$ values exhibited greater variability
284 between baseflow and peak streamflow in GWN than in GUN. From baseflow to approximately peak
285 streamflow, $\delta^{18}\text{O}-\text{H}_2\text{O}$ shifted by an absolute average of 2.1 ‰ at GWN but only 0.6 ‰ at GUN (Table
286 S2). These shifts correspond to an average event-water fraction at peak storm discharge of 0.75 ± 0.13 at
287 GWN and 0.27 ± 0.23 at GUN (Table S2). Event-water fraction uncertainty was relatively large for
288 several events due to small separation between $\delta^{18}\text{O}-\text{H}_2\text{O}$ end members. For example, rainfall and pre-
289 event baseflow end members were separated by only 0.5 ‰ during the 7/22/19 event at GUN, resulting
290 in uncertainty of event-water fractions exceeding 1 (Tables S1 and S2).

291 Storms events have an outsized impact, relative to baseflow, on NO_3^- export at GWN, as
292 indicated by $DF > 1$ for 7 of 8 sampled events (mean = 2.6 ± 0.4 ; Figure 2). The opposite relationship
293 was observed for NO_3^- at GWN ($DF \leq 1$ for all sampled events, mean = 0.5 ± 0.1) indicating that
294 baseflow has an outsized impact on NO_3^- loads relative to storm events. Conversely, DF values at
295 GUN were approximately 1 for both NO_3^- (mean = 1.1 ± 0.2) and NO_3^- (mean = 1.0 ± 0.1),
296 indicating that neither baseflow nor stormflow disproportionately impacted stream NO_3^- loads (Figure
297 2). Event-water fractions were positively, though not significantly, related to DF of NO_3^- ($\tau = 0.32$,
298 $p = 0.09$) and negatively related to DF of NO_3^- across both watersheds (Figure 4; $\tau = -0.32$, $p < 0.05$).
299 In GWN, the total rainfall depth for a given event was positively correlated with the fraction of deposited
300 NO_3^- that was exported in streamwater during the same event ($\tau = 0.74$, $p < 0.05$), but there was no
301 relationship for GUN (Figure 5). Additionally, there was a 1:1 relationship between the event NO_3^-
302 deposition on impervious surfaces and the event NO_3^- streamwater export at GWN ($r^2 = 0.55$, $p <$
303 0.05), but not at GUN (Figure 6). NO_3^- load estimates using traditional methods (concentration from
304 a single grab sample multiplied by mean daily discharge) were biased (range = $-197\% - 123\%$, median
305 absolute value = 36%) relative to NO_3^- load estimates using the multiple samples we collected across
306 the storm hydrograph for the two events that encompassed a full day.

307 **4 Discussion**

308 Hydrologic effects of impervious surfaces likely drive the disproportionate impact of storm
309 events on NO_3^- , and of baseflow on NO_3^- , in the more developed watershed (GWN). Impervious
310 surfaces increase peak storm runoff (Arnold and Gibbons, 1996; Walsh et al., 2005), but differences in
311 peak discharge alone are not the sole explanation for the contrasting results of DF for NO_3^- and
312 NO_3^- between the watersheds. Sampled events with overlapping f_{Runoff} between sites (i.e., similar x-
313 axis values on Figure 2) indicate that the difference between f_{NO_3} for NO_3^- and NO_3^- is much
314 greater at the more developed (GWN) than the less developed watershed (GUN; i.e., different y-axis values on
315 Figure 2). Thus, it is the overland routing of rainfall, and NO_3^- dissolved therein, that likely
316 contributes to the outsized impact of storm events on NO_3^- in the developed watershed. Although
317 both watersheds show a positive relationship between event-water fractions and DF of NO_3^- ($p =$

318 0.09, Figure 4), event-water fractions are much greater in the more developed watershed, GWN (green
319 triangles in Figure 4). Higher event-water fractions promote greater export of $\text{NO}_3^-_{\text{Atm}}$ by reducing the
320 potential for biological processing or retention. Our results provide evidence (i.e., increased event-water
321 fractions, proportional streamwater export of impervious $\text{NO}_3^-_{\text{Atm}}$ deposition) for the mechanism (i.e.,
322 direct routing of rainfall $\text{NO}_3^-_{\text{Atm}}$ to streams) that generates increased $\text{NO}_3^-_{\text{Atm}}$ export in more developed
323 watersheds, which thus expands on previous research demonstrating that more developed watersheds
324 export relatively more $\text{NO}_3^-_{\text{Atm}}$ (Buda and DeWalle, 2009; Burns et al., 2009; Kaushal et al., 2011;
325 Bostic et al., 2021).

326 Our study collected samples across the storm hydrograph and measured $\Delta^{17}\text{O}$ of NO_3^- , which
327 provided a more accurate load estimates of, and insights into, storm $\text{NO}_3^-_{\text{Atm}}$ export than $\delta^{18}\text{O}$ of NO_3^- .
328 For example, estimates of daily $\text{NO}_3^-_{\text{Atm}}$ loads were biased by a median absolute value of 36% using
329 standard methods (i.e., daily average discharge multiplied by $\text{NO}_3^-_{\text{Atm}}$ concentration, estimated using
330 $\Delta^{17}\text{O}$, of a single grab sample; Tsunogai et al., 2014; Rose et al., 2015b; Nakagawa et al., 2018) when
331 compared to “true” daily loads calculated using samples collected across the storm hydrograph from two
332 events that encompassed a full day. Additionally, use of $\Delta^{17}\text{O}$ generally provides more certain estimates
333 of $\text{NO}_3^-_{\text{Atm}}$ fractions and concentrations than $\delta^{18}\text{O}$ because biological processing (e.g., assimilation,
334 denitrification) can change the $\delta^{18}\text{O}$ of NO_3^- and generate large uncertainty ($\pm \sim 30\%$, Kendall et al.,
335 2007) in the $\delta^{18}\text{O}$ - $\text{NO}_3^-_{\text{Terr}}$ end-member and ultimately estimates of $\text{NO}_3^-_{\text{Atm}}$ (Tsunogai et al., 2016).
336 $\Delta^{17}\text{O}$ of NO_3^- , due to its mass-independent fractionation origin, is not subject to the same variability
337 associated with biological processing as $\delta^{18}\text{O}$, thereby decreasing uncertainty in $\text{NO}_3^-_{\text{Atm}}$ estimates
338 (Young et al., 2002; Michalski et al., 2004; Kendall et al., 2007). Indeed, average event $\text{NO}_3^-_{\text{Atm}}$ fractions
339 (i.e., $\frac{\text{NO}_3^-_{\text{Atm}}}{\text{NO}_3^-_{\text{Total}}}$) would have been underestimated by an average of 3% (range = 0 – 7 %) at both sites if
340 using $\delta^{18}\text{O}$ - NO_3^- only (Figure S4), but with a greater effect at the more developed site (GWN). An
341 average underestimate of 3% may appear minor, but it is notable considering that event $\text{NO}_3^-_{\text{Atm}}$
342 fractions averaged 2% and 10% in the less and more developed watersheds, respectively. Increased
343 accuracy of $\text{NO}_3^-_{\text{Atm}}$ export during storm events combined with the *DF* conceptual framework (Figure
344 2) provides a relatively simple means of assessing whether storm events or baseflow have an outsized

345 impact on NO_3^- source export. More accurate estimates of NO_3^- $_{\text{Atm}}$ export also allow for more
346 quantitative investigations into the role of impervious surfaces in routing event rainfall NO_3^- $_{\text{Atm}}$ to
347 streams.

348 Impervious areas in the developed watershed are effective conduits of NO_3^- $_{\text{Atm}}$ to surface
349 waters, as demonstrated by the approximately proportional relationship between event streamwater
350 NO_3^- $_{\text{Atm}}$ export and event NO_3^- $_{\text{Atm}}$ deposition on impervious surfaces (Figure 6). This relationship
351 provides evidence, in addition to higher event-water fractions (Figure 4), for the mechanism of
352 impervious surfaces enhancing export of NO_3^- $_{\text{Atm}}$ during storm events. The 1:1 correspondence of this
353 relationship is surprising, however. For 100% of rainfall NO_3^- $_{\text{Atm}}$ on impervious surfaces to be exported
354 as streamwater during a given event (i.e., 1:1 relationship), all impervious area in the watershed would
355 have to be hydrologically connected to surface waters (i.e., effective impervious areas; Shuster et al.,
356 2005). In a mesoscale (84 km²) and heterogeneous watershed such as GWN, the total impervious area is
357 not equivalent to effective impervious area. Rather, many impervious surfaces drain onto pervious
358 surfaces, or are “ineffective” at directly routing precipitation to channels (Walesh, 1989; but we note
359 that certain pervious surfaces, such as reclaimed mine lands, effectively function as impervious, e.g.,
360 Negley and Eshleman 2006). It is likely that the observed 1:1 relationship (Figure 6) is additionally
361 affected by flushing of dry NO_3^- $_{\text{Atm}}$ deposition from effective impervious areas. Dry NO_3^- deposition,
362 similar to wet deposition, inherits positive $\Delta^{17}\text{O}$ values (~15 – 30 ‰; Nelson et al., 2018) and is generally
363 higher in urban relative to rural areas both locally (Lovett et al., 2000; Bettez and Groffman, 2013) and
364 globally (Decina et al., 2019). Thus, flushing of dry NO_3^- deposition residing on impervious surfaces
365 (or on surfaces such as leaves that can wash onto impervious surfaces) during storm events could
366 contribute to the 1:1 relationship observed in the more developed watershed (green circles in Figure 6).

367 $\Delta^{17}\text{O}$ of NO_3^- can additionally be used to “correct” $\delta^{15}\text{N}$ and $\delta^{18}\text{O}$ values (eqs. 7 and 8) to better
368 indicate isotope values of terrestrial NO_3^- sources (Dejwakh et al., 2012). Values of both $\delta^{15}\text{N}_{\text{Terr}}$ and
369 $\delta^{18}\text{O}-\text{NO}_3^-$ $_{\text{Terr}}$ during storm events fall within the range of values that are typical of natural “soil” and
370 fertilizer (Kendall et al., 2007), but interestingly, NO_3^- $_{\text{Terr}}$ isotope values decreased during storm events
371 relative to baseflow in both watersheds (though not significantly for $\delta^{15}\text{N}$ in GUN; Figure 3). This shift
372 to lower $\delta^{15}\text{N}_{\text{Terr}}$ and $\delta^{18}\text{O}-\text{NO}_3^-$ $_{\text{Terr}}$ values during storm events may reflect the flushing of less

373 “processed” NO_3^- sources from upper soil horizons (Creed et al., 1996), as processing (e.g.,
374 denitrification) generally leaves the remaining NO_3^- with more positive $\delta^{15}\text{N}$ and $\delta^{18}\text{O}$ values due to
375 biologically-mediated fractionation (Denk et al., 2017). Lower $\delta^{15}\text{N}_{\text{Terr}}$ during storm events relative to
376 baseflow was not statistically significant in the mixed agricultural/forested watershed (GUN), but this
377 was due to a single event in which $\delta^{15}\text{N}_{\text{Terr}}$ increased from baseflow to stormflow. Impervious surfaces
378 in the developed watershed likely reduce flushing of this lower $\delta^{18}\text{O}\text{-NO}_3^-_{\text{Terr}}$ by restricting infiltration,
379 but 30% of this watershed is not “developed” (and a higher percentage contains pervious surfaces), which
380 likely contributes to the similarity in $\text{NO}_3^-_{\text{Terr}}$ isotope patterns between study watersheds. Additionally,
381 relatively lower $\text{NO}_3^-_{\text{Terr}}$ isotope values in storm events could be due to reduced in-stream NO_3^- uptake
382 (e.g., assimilation, denitrification) during periods of elevated discharge (Grimm et al., 2005). Biological
383 NO_3^- uptake generally fractionates against heavier isotopes which increases isotope ratios of the
384 remaining NO_3^- (Kendall et al., 2007). If in-stream NO_3^- uptake rates are reduced during high flows,
385 the resulting effect could contribute to the lower $\text{NO}_3^-_{\text{Terr}}$ isotope values during storm events. Relatively
386 lower $\delta^{18}\text{O}\text{-NO}_3^-_{\text{Terr}}$ values during storm events relative to baseflow, and associated insights into
387 watershed-scale N biogeochemistry, were only realized by using $\Delta^{17}\text{O}$ to “correct” $\delta^{18}\text{O}$ values. Without
388 this correction, $\delta^{18}\text{O}\text{-NO}_3^-$ during storm events is strongly influenced by elevated $\delta^{18}\text{O}$ of $\text{NO}_3^-_{\text{Atm}}$, as
389 shown by the similar patterns between $\Delta^{17}\text{O}$ and “uncorrected” $\delta^{18}\text{O}$ in the more developed watershed
390 (Figure 3).

391 Large inputs and stores of N associated with agricultural activity likely contribute to baseflow
392 and storm events having similar impacts on $\text{NO}_3^-_{\text{Terr}}$ and $\text{NO}_3^-_{\text{Atm}}$ export in the mixed
393 agricultural/forested watershed (GUN). DF s of both $\text{NO}_3^-_{\text{Terr}}$ and $\text{NO}_3^-_{\text{Atm}}$ were approximately 1,
394 indicating that loads are primarily explained by changes in discharge. Nutrients, including NO_3^- ,
395 showing similar patterns (loads explained primarily by discharge) over annual time-scales have been
396 attributed to large stores of NO_3^- associated with agricultural inputs (Basu et al., 2010; Thompson et al.,
397 2011). With significant agricultural land-use, both currently (41.3% in 2016; Table 1) and historically
398 (~58% in 1960; O’Bryan and McAvoy, 1966), and consistently high NO_3^- concentrations in
399 streamwater, GUN likely has large stores of NO_3^- in soil and groundwater. Interestingly, our results
400 demonstrate the control of discharge on $\text{NO}_3^-_{\text{Terr}}$ and $\text{NO}_3^-_{\text{Atm}}$ loads over storm-event time scales,

401 suggesting that large reservoirs of NO_3^- contribute to streamwater export of nutrients across varied flow
402 conditions and not just baseflow.

403 The combination of our results with projections of increasing frequency of intense precipitation
404 events (Najjar et al., 2010; Walsh et al., 2014) and increasing urban and suburban sprawl (Jantz et al.,
405 2005; Seto et al., 2012) suggest that $\text{NO}_3^-_{\text{Atm}}$ may become a relatively more important NO_3^- source to
406 downstream waters, assuming no change in NO_3^- deposition rates. This assumption may not be valid
407 everywhere, however; for example, NO_3^- deposition is declining locally (i.e., mid-Atlantic USA; Li et
408 al., 2016) but increasing across many regions (i.e., east Asia; Liu et al., 2013). In our more developed
409 watershed, the positive correlation between rainfall and the fraction of deposited NO_3^- exported in
410 streamwater (Figure 5) suggests that large storm events may export proportionally greater fractions of
411 rainfall $\text{NO}_3^-_{\text{Atm}}$ in urbanizing catchments and increased loads of $\text{NO}_3^-_{\text{Atm}}$ to downstream waters. Best
412 management practices in developed watersheds (e.g., stormwater control measures) can mitigate these
413 potential impacts by increasing infiltration of rainfall (and NO_3^- dissolved in rainfall) and reducing
414 hydrologic connectivity of overland flowpaths (i.e., decrease effective impervious areas; Lee and
415 Heaney, 2003; Walsh et al., 2009), both of which may reduce the load of $\text{NO}_3^-_{\text{Atm}}$ and the proportion of
416 “event” water in streams during storm events. Such practices may additionally reduce $\text{NO}_3^-_{\text{Terr}}$ loads by
417 stimulating denitrification (Bettez and Groffman, 2012), but could also increase the importance of
418 baseflow in NO_3^- export due to increased infiltration. Thus, monitoring of both baseflow and storm
419 events is necessary to quantify potential changes and make targeted water-quality management
420 decisions. Finally, best management practices intended to reduce $\text{NO}_3^-_{\text{Atm}}$ loads in developed watersheds
421 via increased infiltration may provide numerous co-benefits, including reduced runoff (Hood et al., 2007)
422 and higher baseflow (Fletcher et al., 2013), both of which could help restore aquatic ecosystems impacted
423 by urbanization (Walsh et al., 2005).

424 **5. Conclusion**

425 We found that stormflow has a disproportionately large impact on $\text{NO}_3^-_{\text{Atm}}$ export whereas
426 baseflow has a disproportionately small impact on $\text{NO}_3^-_{\text{Terr}}$ export in a moderately developed watershed.
427 In contrast, neither stormflow nor baseflow have an outsized impact on $\text{NO}_3^-_{\text{Atm}}$ or $\text{NO}_3^-_{\text{Terr}}$ export in a

428 mixed land-use watershed with significant agriculture. Hydrologic connectivity of overland flow paths
429 associated with impervious surfaces likely promote rapid transport of $\text{NO}_3^-_{\text{Atm}}$ to streams during storm
430 events in the more developed watershed, with higher rainfall storms exporting a greater fraction of
431 deposited NO_3^- than lower rainfall events and event $\text{NO}_3^-_{\text{Atm}}$ streamwater export approximately
432 equaling rainfall $\text{NO}_3^-_{\text{Atm}}$ on impervious surfaces. Large reserves of new and/or legacy agricultural-
433 associated nitrogen in soils in the mixed land-use watershed likely influenced the similar response of
434 $\text{NO}_3^-_{\text{Atm}}$ or $\text{NO}_3^-_{\text{Terr}}$ to stormflow and baseflow.

435 **Appendices**

436 Not applicable.

437 **Code availability**

438 Not applicable.

439 **Data availability**

440 [Complete data is presented in Tables S4 and S5.](#)

441 **Author contributions**

442 DMN and KNE: Conceptualization, Methodology, Writing – Review and Editing, Supervision, Funding
443 Acquisition

444 JTB: Conceptualization, Methodology, Investigation, Formal Analysis, Writing – Original Draft,
445 Writing – Review and Editing, Visualization, Funding Acquisition

Acknowledgements

Thanks to Pavithra Pitumpe Arachchige and Jim Garlitz for NO_3^- concentration analysis. Robert Hirsch of the U.S. Geological Survey provided guidance on WRTDS-K and R scripts for estimating $\text{NO}_{3\text{-Total}}$ uncertainty. DMN, KNE, and JTB received support from Maryland Sea Grant under award NA14OAR4170090 R/WS-3 from the National Oceanic and Atmospheric Administration, U.S. Department of Commerce. JTB received support from Maryland Sea Grant under award SA75281900-A from the National Oceanic and Atmospheric Administration, U.S. Department of Commerce. This material is based upon work supported by the National Science Foundation Graduate Research Fellowship (to JTB) under Grant No. 1840380. Any opinion, findings, conclusions, recommendations expressed in this material are those of the authors and do not necessarily reflect the views of the National Science Foundation.

References

Arnold CL, Gibbons CJ. 1996. Impervious surface coverage: The emergence of a key environmental indicator. *Journal of the American Planning Association* 62: 243-258. <https://doi.org/10.1080/01944369608975688>

Barnes RT, Raymond PA. 2010. Land-use controls on sources and processing of nitrate in small watersheds: Insights from dual isotopic analysis. *Ecological Applications* 20: 1961-1978. <https://doi.org/10.1890/08-1328.1>

Basu NB, Destouni G, Jawitz JW, Thompson SE, Loukinova NV, Darracq A, Zanardo S, Yaeger M, Sivapalan M, Rinaldo A, Rao PSC. 2010. Nutrient loads exported from managed catchments reveal emergent biogeochemical stationarity. *Geophysical Research Letters* 37. <https://doi.org/10.1029/2010GL045168>

Bettez N, Groffman P. 2012. Denitrification potential in stormwater control structures and natural riparian zones in an urban landscape. *Environmental Science & Technology* 46 20: 10909-10917. <https://doi.org/10.1021/es301409z>

Bettez ND, Groffman PM. 2013. Nitrogen deposition in and near an urban ecosystem. *Environmental Science & Technology* 47: 6047-6051. <https://doi.org/10.1021/es400664b>

Böhlke JK, Mroczkowski SJ, Coplen TB. 2003. Oxygen isotopes in nitrate: New reference materials for $^{18}\text{O}:^{17}\text{O}:^{16}\text{O}$ measurements and observations on nitrate-water equilibration. *Rapid Communications in Mass Spectrometry* 17: 1835-1846. <https://doi.org/10.1002/rcm.1123>

Bonnin GM, Martin D, Lin B, Parzybok T, Yekta M, Riley D. 2004. Precipitation-frequency atlas of the United States. Volume 2 version 3.0. Delaware, District of Columbia, Illinois, Indiana, Kentucky, Maryland, New Jersey, North Carolina, Ohio, Pennsylvania, South Carolina, Tennessee, Virginia, West Virginia.

Bostic JT, Nelson DM, Sabo RD, Eshleman KN. 2021. Terrestrial nitrogen inputs affect the export of unprocessed atmospheric nitrate to surface waters: Insights from triple oxygen isotopes of nitrate. *Ecosystems*. <https://doi.org/10.1007/s10021-021-00722-9>

Buda AR, DeWalle DR. 2009. Dynamics of stream nitrate sources and flow pathways during stormflows on urban, forest and agricultural watersheds in central Pennsylvania, USA. *Hydrological Processes* 23: 3292-3305. <https://doi.org/10.1002/hyp.7423>

Burns DA, Boyer EW, Elliott EM, Kendall C. 2009. Sources and transformations of nitrate from streams draining varying land uses: Evidence from dual isotope analysis. *Journal of Environmental Quality* 38: 1149-1159. [10.2134/jeq2008.0371](https://doi.org/10.2134/jeq2008.0371)

Camargo JA, Alonso Á. 2006. Ecological and toxicological effects of inorganic nitrogen pollution in aquatic ecosystems: A global assessment. *Environment International* 32: 831-849. <https://doi.org/10.1016/j.envint.2006.05.002>

Casciotti KL, Sigman DM, Hastings MG, Böhlke J, Hilkert A. 2002. Measurement of the oxygen isotopic composition of nitrate in seawater and freshwater using the denitrifier method. *Analytical Chemistry* 74: 4905-4912. <https://doi.org/10.1021/ac020113w>

Chesapeake Bay Program. 2019. Chesapeake assessment and scenario tool (CAST). Chesapeake Bay Program Office. Chesapeake Bay Program. 2021. Chesapeake Bay Program Water Quality Database, 1984-present. Accessed March 1, 2021 from http://www.chesapeakebay.net/data/downloads/cbp_water_quality_database_1984_present.

Chanat JG, Moyer DL, Blomquist JD, Hyer KE, Langland MJ. 2016. Application of a weighted regression model for reporting nutrient and sediment concentrations, fluxes, and trends in concentration and flux for the Chesapeake Bay nontidal water-quality monitoring network, results through water year 2012. *Scientific Investigations Report*. Reston, VA, p88. <https://doi.org/10.3133/sir20155133>

Cook PG, Herczeg AL. 2012. *Environmental tracers in subsurface hydrology*: Springer Science & Business Media. <https://doi.org/10.1007/978-1-4615-4557-6>

Creed IF, Band LE, Foster NW, Morrison IK, Nicolson JA, Semkin RS, Jeffries DS. 1996. Regulation of nitrate-N release from temperate forests: A test of the N flushing hypothesis. *Water Resources Research* 32: 3337-3354. <https://doi.org/10.1029/96WR02399>

DeCicco LA, Lorenz, D., Hirsch, R.M. 2018. dataRetrieval: R packages for discovering and retrieving water data available from U.S. Federal hydrologic web services. United States Geological Survey. 10.5066/P9X4L3GE

Decina SM, Hutyla LR, Templer PH. 2019. Hotspots of nitrogen deposition in the world's urban areas: A global data synthesis. *Frontiers in Ecology and the Environment* 18: 92-100. <https://doi.org/10.1002/fee.2143>

Dejwakh NR, Meixner T, Michalski G, McIntosh J. 2012. Using ^{17}O to investigate nitrate sources and sinks in a semi-arid groundwater system. *Environmental Science & Technology* 46: 745-751. <https://doi.org/10.1021/es203450z>

Denk TRA, Mohn J, Decock C, Lewicka-Szczebak D, Harris E, Butterbach-Bahl K, Kiese R, Wolf B. 2017. The nitrogen cycle: A review of isotope effects and isotope modeling approaches. *Soil Biology and Biochemistry* 105: 121-137. <https://doi.org/10.1016/j.soilbio.2016.11.015>

Dingman SL. 1994. *Physical hydrology*. xii, 643 pp.

Divers, MT, Elliott, EM, Bain, DJ. Quantification of nitrate sources to an urban stream using dual nitrate isotopes. *Environmental Science & Technology*, 48: 10580-10587. <https://doi.org/10.1021/es404880j>

Edmund M. Hart and Kendon Bell. 2015. PRISM: Download data from the Oregon PRISM project.

Elliott EM, Kendall C, Wankel SD, Burns DA, Boyer EW, Harlin K, Bain DJ, Butler TJ. 2007. Nitrogen isotopes as indicators of NO_x source contributions to atmospheric nitrate deposition across the midwestern and northeastern United States. *Environmental Science & Technology* 41: 7661-7667. <https://doi.org/10.1021/es070898t>

Fenneman NM, Johnson, D.W. 1946. *Physiographic divisions of the conterminus U.S.* U.S. Geological Survey. Reston, VA.

Fletcher, T., Andrieu, H., Hamel, P. 2013. Understanding, management and modelling of urban hydrology and its consequences for receiving waters: A state of the art. *Advances in Water Resources* 51: 261-279. <https://doi.org/10.1016/j.advwatres.2012.09.001>

Genereux D. 1998. Quantifying uncertainty in tracer-based hydrograph separations. *Water Resources Research* 34: 915-919. <https://doi.org/10.1029/98WR00010>

Grimm NB, Sheibley RW, Crenshaw CL, Dahm CN, Roach WJ, Zeglin LH. N retention and transformation in urban streams. 2005. Journal of the North American Benthological Society 24(3): 626-642. <https://doi.org/10.1899/04-027.1>

Huang S, Wang F, Elliott EM, Zhu F, Zhu W, Koba K, Yu Z, Hobbie EA, Michalski G, Kang R, Wang A, Zhu J, Fu S, Fang Y. 2020. Multiyear measurements on $\Delta^{17}\text{O}$ of stream nitrate indicate high nitrate production in a temperate forest. Environmental Science & Technology 54: 4231-4239. <https://doi.org/10.1021/acs.est.9b07839>

Helsel DR, Hirsch RM, Ryberg KR, Archfield SA, Gilroy EJ. 2020. Statistical methods in water resources. Techniques and Methods. Reston, VA, p. 484. <https://doi.org/10.3133/tm4A3>

Homer C, Dewitz J, Jin S, Xian G, Costello C, Danielson P, Gass L, Funk M, Wickham J, Stehman S, Auch R, Riitters K. 2020. Conterminous united states land cover change patterns 2001–2016 from the 2016 national land cover database. ISPRS Journal of Photogrammetry and Remote Sensing 162: 184-199. <https://doi.org/10.1016/j.isprsjprs.2020.02.019>

Hood, M., Clausen, J., Warner, G. 2007. Comparison of stormwater lag times for low impact and traditional residential development. Journal of the American Water Resources Association 43: 1036-1046. <https://doi.org/10.1111/j.1752-1688.2007.00085.x>

IAEA. 1995. Reference and intercomparison materials for stable isotopes of light elements. Vienna: International Atomic Energy Agency.

Jantz P, Goetz S, Jantz C. 2005. Urbanization and the loss of resource lands in the Chesapeake Bay watershed. Environmental Management 36: 808-825. <https://doi.org/10.1007>

Jarvis NJ. 2020. A review of non-equilibrium water flow and solute transport in soil macropores: Principles, controlling factors and consequences for water quality. European Journal of Soil Science 71: 279-302. <https://doi.org/10.1111/j.1365-2389.2007.00915.x>

Kaiser J, Hastings MG, Houlton BZ, Röckmann T, Sigman DM. 2007. Triple oxygen isotope analysis of nitrate using the denitrifier method and thermal decomposition of N_2O . Analytical Chemistry 79: 599-607. <https://doi.org/10.1021/ac061022s>

Kaushal SS, Groffman PM, Band LE, Elliott EM, Shields CA, Kendall C. 2011. Tracking nonpoint source nitrogen pollution in human-impacted watersheds. Environmental Science & Technology 45: 8225-8232. <https://doi.org/10.1021/es200779e>

Kemp WM, Boynton WR, Adolf JE, Boesch DF, Boicourt WC, Brush G, Cornwell JC, Fisher TR, Glibert PM, Hagy JD. 2005. Eutrophication of Chesapeake Bay: Historical trends and ecological interactions. *Marine Ecology Progress Series* 303: 1-29. <https://doi.org/10.3354/meps303001>

Kendall C, Elliott, E, Wankel, S. 2007. *Tracing anthropogenic inputs of nitrogen to ecosystems*: Blackwell Publishing. <https://doi.org/10.1002/9780470691854.ch12>

Kincaid DW, Seybold EC, Adair EC, Bowden WB, Perdrial JN, Vaughan MCH, Schroth AW. 2020. Land use and season influence event-scale nitrate and soluble reactive phosphorus exports and export stoichiometry from headwater catchments. *Water Resources Research* 56. <https://doi.org/10.1029/2020WR027361>

Klaus J, McDonnell J. 2013. Hydrograph separation using stable isotopes: Review and evaluation. *Journal of Hydrology* 505: 47-64. <https://doi.org/10.1016/j.jhydrol.2013.09.006>

Kottek M, Grieser J, Beck C, Rudolf B, Rubel F. 2006. World map of the Köppen-Geiger climate classification updated. *Meteorologische Zeitschrift* 15: 259-263. <https://doi.org/10.1127/0941-2948/2006/0130>.

Lee JG, Heaney JP. 2003. Estimation of urban imperviousness and its impacts on storm water systems. *Journal of Water Resources Planning and Management* 129: 419-426. [https://doi.org/10.1061/\(ASCE\)0733-9496\(2003\)129:5\(419\)](https://doi.org/10.1061/(ASCE)0733-9496(2003)129:5(419))

Lefcheck JS, Orth RJ, Dennison WC, Wilcox DJ, Murphy RR, Keisman J, Gurbisz C, Hannam M, Landry JB, Moore KA. 2018. Long-term nutrient reductions lead to the unprecedented recovery of a temperate coastal region. *Proceedings of the National Academy of Sciences* 115: 3658-3662. <https://doi.org/10.1073/pnas.1715798115>

Li Y, Schichtel BA, Walker JT, Schwede DB, Chen X, Lehmann CM, Puchalski MA, Gay DA, Collett JL. 2016. Increasing importance of deposition of reduced nitrogen in the United States. *Proceedings of the National Academy of Sciences* 113: 5874-5879. <https://doi.org/10.1073/pnas.1525736113>

Liu, X., Zhang, Y., Wenxuan, H., Tang, A., Shen, J., Cui, Z., Vitousek, P., Erismann, J., Goudling, K., Christie, P., Fangmeier, A., Zhang, F. 2013. Enhanced nitrogen deposition over China. *Nature* 494: 459-462. <https://doi.org/10.1038/nature11917>

Lovett GM, Traynor MM, Pouyat RV, Carreiro MM, Zhu W-X, Baxter JW. 2000. Atmospheric deposition to oak forests along an urban-rural gradient. *Environmental Science & Technology* 34: 4294-4300. <https://doi.org/10.1021/es001077q>

- McGuire K, McDonnell J. 2007. Stable isotope tracers in watershed hydrology. *Stable isotopes in ecology and environmental science*, p334-374. <https://doi.org/10.1002/9780470691854.ch11>
- Michalski G, Meixner T, Fenn M, Hernandez L, Sirulnik A, Allen E, Thiemens M. 2004. Tracing atmospheric nitrate deposition in a complex semiarid ecosystem using $\Delta^{17}\text{O}$. *Environmental Science & Technology* 38: 2175-2181. <https://doi.org/10.1021/es034980+>
- Michalski G, Savarino J, Böhlke JK, Thiemens M. 2002. Determination of the total oxygen isotopic composition of nitrate and the calibration of a $\Delta^{17}\text{O}$ nitrate reference material. *Analytical Chemistry* 74: 4989-4993. <https://doi.org/10.1021/ac0256282>
- Michalski G, Scott Z, Kabling M, Thiemens MH. 2003. First measurements and modeling of $\Delta^{17}\text{O}$ in atmospheric nitrate. *Geophysical Research Letters* 30. <https://doi.org/10.1029/2003GL017015>
- Najjar RG, Pyke CR, Adams MB, Breitburg D, Hershner C, Kemp M, Howarth R, Mulholland MR, Paolisso M, Secor D, Sellner K, Wardrop D, Wood R. 2010. Potential climate-change impacts on the Chesapeake Bay. *Estuarine, Coastal and Shelf Science* 86: 1-20. <https://doi.org/10.1016/j.ecss.2009.09.026>
- Nakagawa F, Tsunogai U, Obata Y, Ando K, Yamashita N, Saito T, Uchiyama S, Morohashi M, Sase H. 2018. Export flux of unprocessed atmospheric nitrate from temperate forested catchments: A possible new index for nitrogen saturation. *Biogeosciences* 15: 7025-7042. <https://doi.org/10.5194/bg-15-7025-2018>
- Negley, T.L. and Eshleman, K.N. 2006. Comparison of stormflow responses of surface-mined and forested watersheds in the Appalachian Mountains, USA. *Hydrological Processes* 20: 3467-3483. <https://doi.org/10.1002/hyp.6148>
- Nelson DM, Tsunogai U, Ding D, Ohyama T, Komatsu DD, Nakagawa F, Noguchi I, Yamaguchi T. 2018. Triple oxygen isotopes indicate urbanization affects sources of nitrate in wet and dry atmospheric deposition. *Atmospheric Chemistry and Physics* 18: 6381-6392. <https://doi.org/10.5194/acp-18-6381-2018>
- NRC. 2000. *Clean coastal waters: Understanding and reducing the effects of nutrient pollution*. Washington, DC: The National Academies Press. 428p. <https://doi.org/10.17226/9812>
- O'Bryan, D., and McAvoy, R.L. 1966. *Gunpowder Fall Maryland: Uses of a water resource today and tomorrow*. Geological Survey Water-Supply Paper 1815.
- Paul MJ, Meyer JL. 2001. Streams in the urban landscape. *Annual Review of Ecology and Systematics* 32: 333-365. <https://doi.org/10.1146/annurev.ecolsys.32.081501.114040>

PRISM Climate Group, Oregon State University, <https://prism.oregonstate.edu>, data created 4 Feb 2014, accessed 16 Dec 2020.

R Development Core Team. 2019. R: A language and environment for statistical computing. Vienna, Austria: R Foundation for Statistical Computing.

Rose LA, Sebestyen SD, Elliott EM, Koba K. 2015a. Drivers of atmospheric nitrate processing and export in forested catchments. *Water Resources Research* 51: 1333-1352. <https://doi.org/10.1002/2014WR015716>

Rose LA, Elliott EM, Adams MB. 2015b. Triple nitrate isotopes indicate differing nitrate source contributions to streams across a nitrogen saturation gradient. *Ecosystems* 18: 1209-1223. <https://doi.org/10.1007/s10021-015-9891-8>

Sabo, RD, Nelson, DM, Eshleman, KN. Episodic, seasonal, and annual export of atmospheric and microbial nitrate from a temperate forest. *Geophysical Research Letters*, 43, 2: 683-691. <https://doi.org/10.1002/2015gl066758>

Seto KC, Guneralp B, Hutyra LR. 2012. Global forecasts of urban expansion to 2030 and direct impacts on biodiversity and carbon pools. *Proceedings of the National Academy of Sciences* 109: 16083-16088. <https://doi.org/10.1073/pnas.1211658109>

Shuster WD, Bonta J, Thurston H, Warnemuende E, Smith DR. 2005. Impacts of impervious surface on watershed hydrology: A review. *Urban Water Journal* 2: 263-275. <https://doi.org/10.1080/15730620500386529>

Sigman DM, Casciotti KL, Andreani M, Barford C, Galanter M, Böhlke J. 2001. A bacterial method for the nitrogen isotopic analysis of nitrate in seawater and freshwater. *Analytical Chemistry* 73: 4145-4153. <https://doi.org/10.1021/ac010088e>

Sklash M, Farvolden R, Fritz P. 1976. A conceptual model of watershed response to rainfall, developed through the use of oxygen-18 as a natural tracer. *Canadian Journal of Earth Sciences* 13: 271-283. <https://doi.org/10.1139/e76-02>

Steffen W, Richardson K, Rockström J, Cornell SE, Fetzer I, Bennett EM, Biggs R, Carpenter SR, Vries Wd, Wit CAd, Folke C, Gerten D, Heinke J, Mace GM, Persson LM, Ramanathan V, Reyers B, Sörlin S. 2015. Planetary boundaries: Guiding human development on a changing planet. *Science* 347: 6219. <https://doi.org/10.1126/science.1259855>

Stevens CJ. 2019. Nitrogen in the environment. *Science* 363: 578-580. <https://doi.org/10.1126/science.aav8215>

Thompson SE, Basu NB, Lascrain Jr. J, Aubeneau A, Rao PSC. 2011. Relative dominance of hydrologic versus biogeochemical factors on solute export across impact gradients. *Water Resources Research* 47. <https://doi.org/10.1029/2010WR009605>

Tsunogai U, Komatsu DD, Ohyama T, Suzuki A, Nakagawa F, Noguchi I, Takagi K, Nomura M, Fukuzawa K, Shibata H. 2014. Quantifying the effects of clear-cutting and strip-cutting on nitrate dynamics in a forested watershed using triple oxygen isotopes as tracers. *Biogeosciences* 11: 5411-5424. <https://doi.org/10.5194/bg-11-5411-2014>

Tsunogai U, Miyauchi T, Ohyama T, Komatsu DD, Nakagawa F, Obata Y, Sato K, Ohizumi T. 2016. Accurate and precise quantification of atmospheric nitrate in streams draining land of various uses by using triple oxygen isotopes as tracers. *Biogeosciences* 13: 3441-3459. <https://doi.org/10.5194/bg-13-3441-2016>

U.S. Geological Survey, 2022, National Water Information System data available on the World Wide Web (USGS Water Data for the Nation), accessed [June 20, 2022], at URL [<https://waterdata.usgs.gov/usa/nwis/uv?01589300> and https://waterdata.usgs.gov/md/nwis/uv/?site_no=01582500]

Vaughan MCH, Bowden WB, Shanley JB, Vermilyea A, Sleeper R, Gold AJ, Pradhanang SM, Inamdar SP, Levia DF, Andres AS, Birgand F, Schroth AW. 2017. High-frequency dissolved organic carbon and nitrate measurements reveal differences in storm hysteresis and loading in relation to land cover and seasonality. *Water Resources Research* 53: 5345-5363. <https://doi.org/10.1002/2017WR020491>

Walesh SG. 1989. Fundamentals of urban surface water management. *Urban surface water management*, p1-51. <https://doi.org/10.1002/9780470172810.ch1>

Walsh CJ, Fletcher TD, Ladson AR. 2009. Retention capacity: A metric to link stream ecology and storm-water management. *Journal of Hydrologic Engineering* 14: 399-406. [https://doi.org/10.1061/\(ASCE\)1084-0699\(2009\)14:4\(399\)](https://doi.org/10.1061/(ASCE)1084-0699(2009)14:4(399))

Walsh CJ, Roy AH, Feminella JW, Cottingham PD, Groffman PM, Morgan RP. 2005. The urban stream syndrome: Current knowledge and the search for a cure. *Journal of the North American Benthological Society* 24: 706-723. <https://doi.org/10.1899/04-028.1>

Walsh J, Wuebbles D, Hayhoe K, Kossin J, Kunkel K, Stephens G, Thorne P, Vose R, Wehner M, Willis J, Anderson D, Doney S, Feely R, Hennon P, Kharin V, Knutson T, Landerer F, Lenton T, Kennedy J, Somerville R editors. 2014. *Our changing climate, climate change impacts in the united states: The third national climate assessment.*

Young ED, Galy A, Nagahara H. 2002. Kinetic and equilibrium mass-dependent isotope fractionation laws in nature and their geochemical and cosmochemical significance. *Geochimica et Cosmochimica Acta* 66: 1095-1104. [https://doi.org/10.1016/S0016-7037\(01\)00832-8](https://doi.org/10.1016/S0016-7037(01)00832-8)

Zhang Q, Blomquist JD, Moyer DL, Chantat JG. 2019. Estimation bias in water-quality constituent concentrations and fluxes: A synthesis for Chesapeake Bay rivers and streams. *Frontiers in Ecology and Evolution* 7. <https://doi.org/10.3389/fevo.2019.00109>

Zhang Q, Hirsch RM. 2019. River water-quality concentration and flux estimation can be improved by accounting for serial correlation through an autoregressive model. *Water Resources Research* 55: 9705-9723. <https://doi.org/10.1029/2019WR025338>

Zhang Q, Murphy RR, Tian R, Forsyth MK, Trentacoste EM, Keisman J, Tango PJ. 2018. Chesapeake Bay's water quality condition has been recovering: Insights from a multimetric indicator assessment of thirty years of tidal monitoring data. *Science of the Total Environment* 637-638: 1617-1625. <https://doi.org/10.1016/j.scitotenv.2018.05.025>

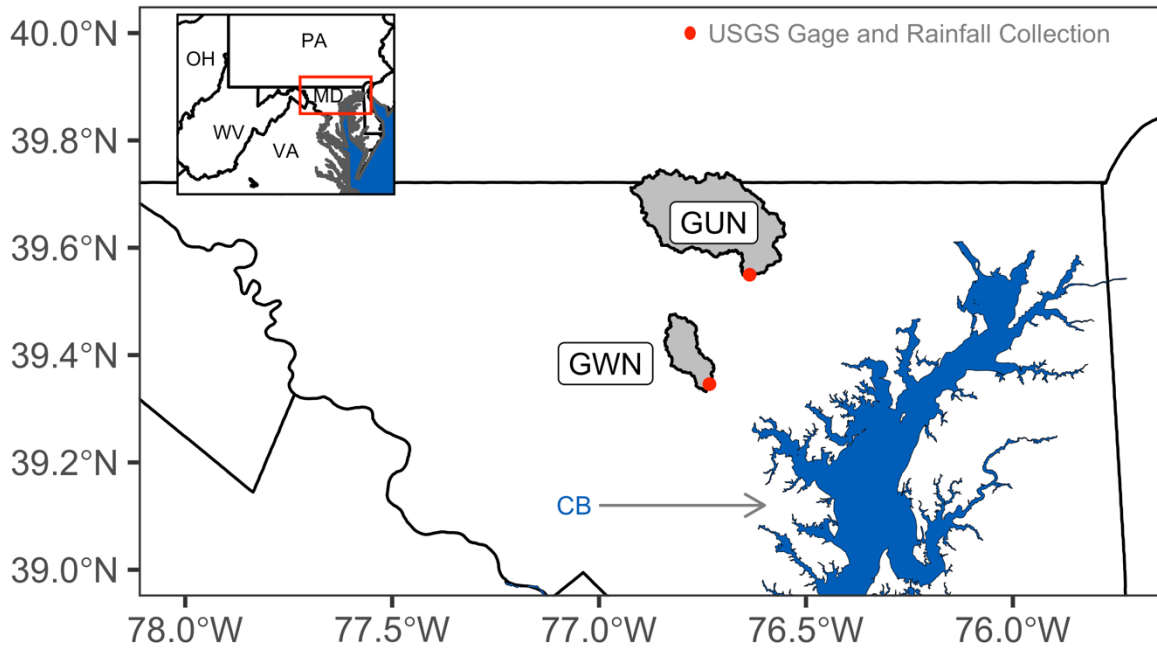
Tables

Table 1. Watershed attributes.

Watershed	Area (ha)	Land-Use (%)				MA T (°C)	MA P (cm)	Lithology (%)		
		Forest	Agriculture	Developed	Impervious			Unconsolidated	Crystalline	Carbonate
Gwynns Falls (GWN)	8400	23.4	5.0	70.1	14.6	12.7	113.5	0	95.1	4.9
Gunpowder Falls (GUN)	4140	45.4	41.3	10.9	0.3	11.9	116.0	0	99.8	0.2

Land-use percentages were calculated from the 2016 National Land Cover Database, impervious is the sum of medium and high intensity developed land-use classes; agricultural land represents the sum of both cultivated crop and pasture/hay land classes (Homer et al., 2020). Land use percentages do not sum to 100% as all land use classes are not listed (e.g. open water, wetlands). MAT = Mean Annual Temperature, MAP = Mean Annual Precipitation. Note that MAT and MAP cover the time period from 1981-2010 (PRISM, 2014). Lithology data were obtained from Zhang et al. 2019.

Figures



5 **Figure 1. Site map showing watershed boundaries (GWN = Gwynns Falls, GUN = Gunpowder Falls), United States Geology Survey (USGS) gaging stations and rainfall collection sites, and Chesapeake Bay (CB) location. Inset map shows relative position of watersheds in Maryland (MD) relative to neighboring states (PA = Pennsylvania, OH = Ohio, WV = West Virginia, VA = Virginia).**

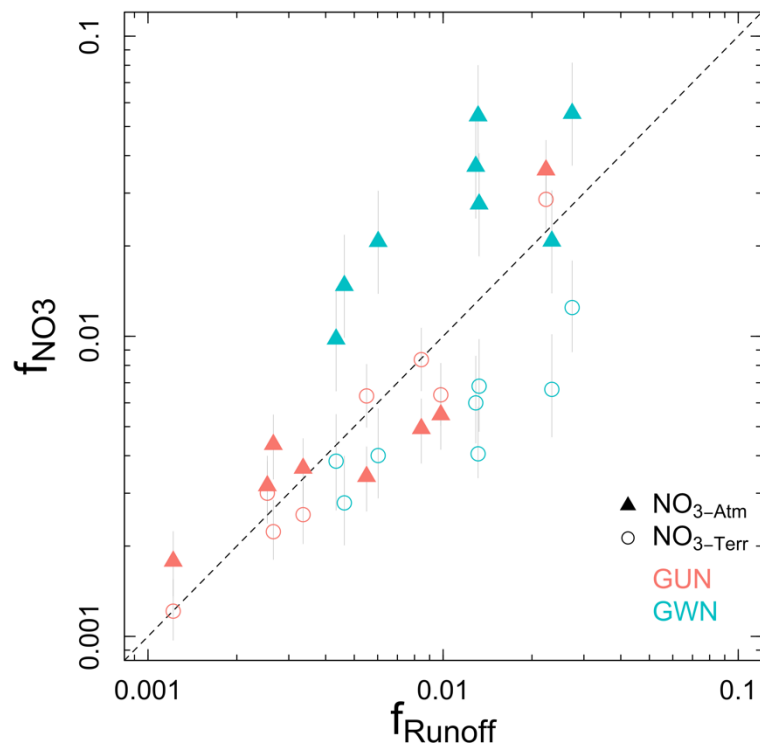
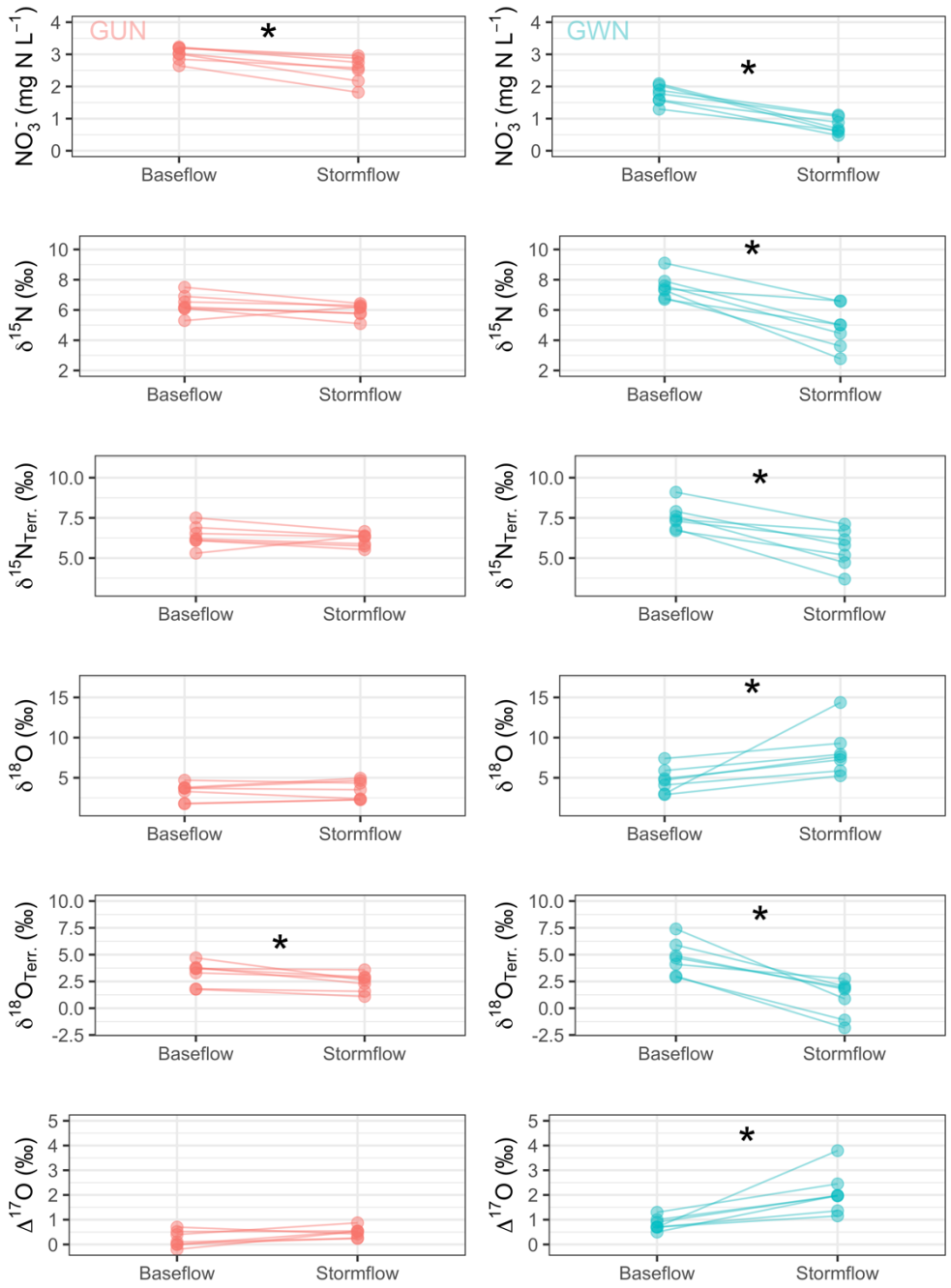
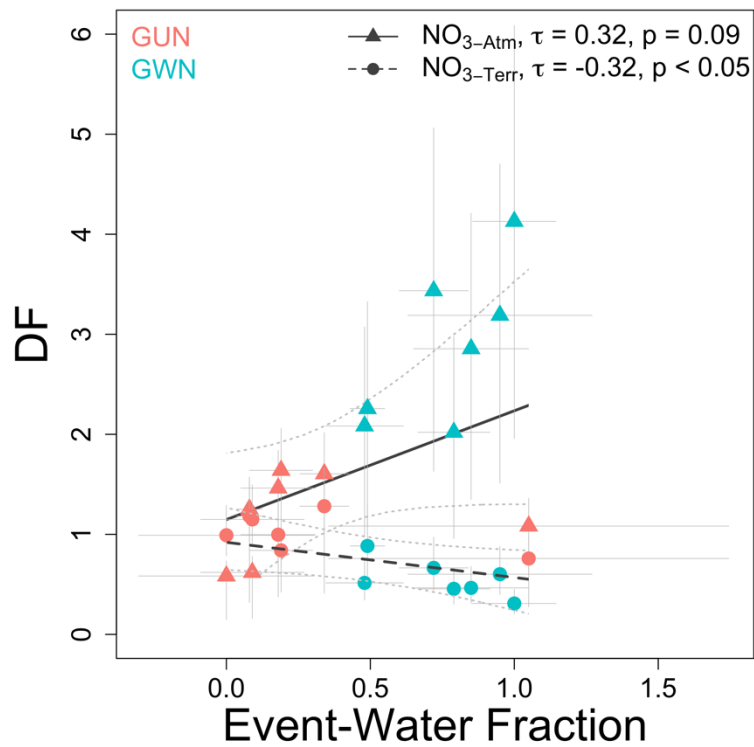


Figure 2. Fraction of NO₃⁻ loads (fNO₃; separated by NO₃⁻Terr, circles, and NO₃⁻Atm, triangles) and discharge (fRunoff) during the study duration (14 months) represented by sampled storm events (n = 8). Points falling above the dashed line (1:1 line) indicate storm events have an outsized impact on NO₃⁻ loads and points falling below the line indicate baseflow has an outsized impact on NO₃⁻ loads. Points on or near the 1:1 line indicate a chemostatic response, in which storms nor baseflow have an outsized impact on NO₃⁻ loads.

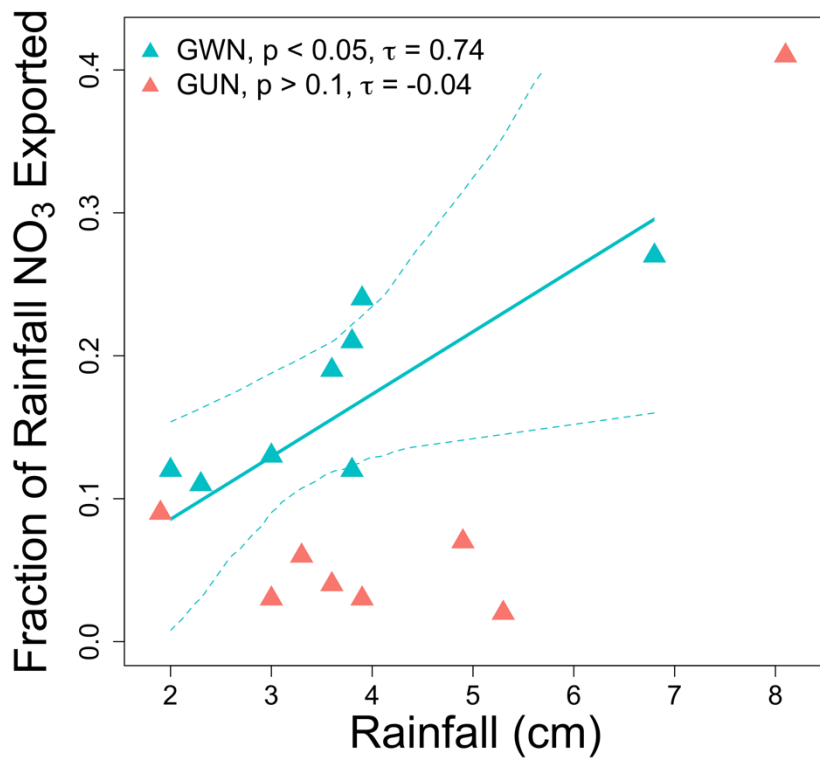
10



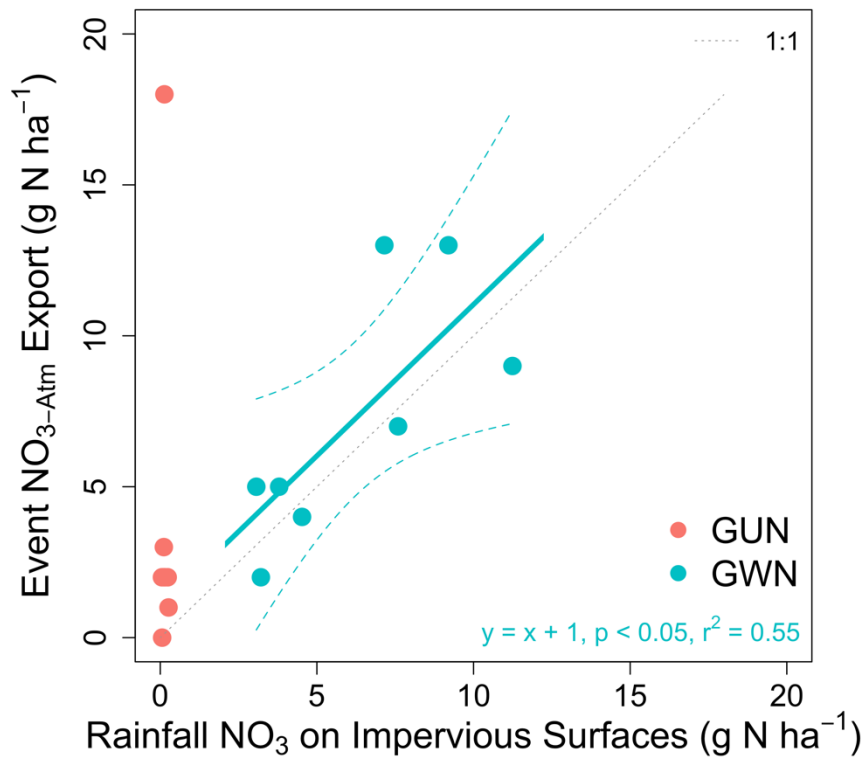
15 **Figure 3.** Event mean NO_3^- concentrations and $\delta^{15}\text{N}$, $\delta^{15}\text{N}_{\text{Terr.}}$, $\delta^{18}\text{O}$, $\delta^{18}\text{O}_{\text{Terr.}}$, and $\Delta^{17}\text{O}$ values of NO_3^- for samples collected during storm events paired with the corresponding baseflow sample preceding the event. Asterisk (*) indicates significant difference at $p < 0.05$ as determined using a Wilcoxon ranked-sum test.



20 **Figure 4. Disproportionality factor (DF) and event-water fraction for $\text{NO}_3^-_{\text{Atm}}$ (triangles) and $\text{NO}_3^-_{\text{Terr}}$ (circles). Event-water fraction and DF are positively, but not significantly correlated for $\text{NO}_3^-_{\text{Atm}}$ ($\tau = 0.32$, $p = 0.09$) while event-water fraction and DF are significantly, negative correlated for $\text{NO}_3^-_{\text{Terr}}$ ($\tau = -0.32$, $p < 0.05$) across both watersheds. The thin, dotted line shows bootstrapped 95% confidence intervals.**



25 Figure 5. The fraction of NO_3^- in rainfall that is exported in streamwater during the same event is positively significantly related with total event rainfall at GWN ($p < 0.05$, $\tau = 0.74$) but not at GUN ($p > 0.1$, $\tau = -0.04$). The solid line is the Theil-Sen slope and the thin, dotted line shows the bootstrapped 95% confidence intervals.



30 Figure 6. The event $\text{NO}_3^-_{\text{Atm}}$ yield (in g N ha^{-1}) has a 1:1 relationship with the estimated rainfall $\text{NO}_3^-_{\text{Atm}}$ deposition on impervious surfaces (in g N ha^{-1}) at GWN (slope = 1.00, intercept = 1, $r^2 = 0.55$, $p < 0.05$), but not at GUN.